Advanced Composites and Hybrid Materials (2026) 9:56
https://doi.org/10.1007/s42114-025-01566-w

RESEARCH

Energy-efficient reservoir computing with 10 × 10 crossbar array memristor for high performance multitask recognition

Faisal Ghafoor[1] · Honggyun Kim[2] · Hui Zhang[3] · Bilal Ghafoor[4] · Myungjae Lee[5] · Tuo Shi[6] · Deok-kee Kim[1,2]

Received: 9 May 2025 / Revised: 16 October 2025 / Accepted: 26 November 2025

Abstract

Memristors hold significant potential for developing energy-efficient artificial intelligence (AI) hardware through parallel in-memory computing, thereby overcoming the long-standing von Neumann bottleneck. However, their widespread adoption is hindered by pronounced cycle-to-cycle (C2C) and device-to-device (D2D) variability. This study presents a novel approach to addressing key challenges in memristor-based artificial intelligence devices. We developed a 10 × 10 crossbar array of $Fe_{50}W_{50}$ hybrid nanocomposite memristors, demonstrating forming-free operation, low variability, and high reliability with low power consumption. The devices exhibit forming-free, low-variability, and highly reliable switching with ultra-low power consumption. The aligned grain boundaries within the nanocomposite enable well-controlled filament formation, ensuring consistent resistive switching characteristics. Leveraging these features, a reservoir computing (RC) architecture is implemented, demonstrating robust performance characterized by 4-bit input separability, short-term (fading) memory, and a strong echo-state property. The system achieves outstanding pattern-recognition accuracies of 98.79% for handwritten character recognition, 88.92% for garment classification, and 91.51% for digit recognition, along with 87.82% accuracy in multi-attribute classification and 98.62% in gesture recognition, underscoring its versatility in spatiotemporal processing. This material algorithm co-design framework not only enhances computational efficiency but also addresses core reliability challenges in memristor-based AI systems, paving the way toward scalable and energy-efficient neuromorphic computing architectures.

Keywords Reservoir computing (RC) · Artificial intelligence (AI) · Neuromorphic systems (NSs) · Grain boundaries (GBs) · Hybrid nanocomposite material (HNM)

Faisal Ghafoor and Honggyun Kim contributed equally to this work.

✉ Deok-kee Kim
deokkeekim@sejong.ac.kr

1 Department of Electrical Engineering, Sejong University, Seoul 05006, Republic of Korea

2 Department of Semiconductor Systems Engineering, Sejong University, Seoul 05006, Republic of Korea

3 College of Information Science and Electronic Engineering, Zhejiang University, Hangzhou 310013, China

4 State Key Laboratory of Advanced Special Steel, School of Materials Science and Engineering, Shanghai University, 99 Shangda Rd, Shanghai 200444, China

5 Institute of conversion, Daegu Gyeongbuk Institute of Science and Technology (DGIST), Daegu 42988, Republic of Korea

6 Research Center for Intelligent Technology Standardization, Zhejiang Lab, Hangzhou 311121, China

1 Introduction

Neuromorphic systems (NSs) leveraging memristive devices are rapidly advancing field focused on emulating the computational efficiency of biological systems for cognitive tasks like pattern and speech recognition. This approach aims to replicate the brain's remarkable capabilities in artificial hardware [1–3]. The majority of organic electronic devices operate on principles analogous to those observed in biological synapses and neurons, namely ion migration. They are capable of effectively emulating synaptic and neuronal properties [4–6]. Additionally, memristors can be arranged in extensive crossbar clusters to facilitate natural weighted vector-matrix multiplication via electrical current summation. This development is highly parallel and demanding for traditional von Neumann systems, making it well-suited for deep learning algorithms [7]. The growing demand for high-performance computing and storage has driven the

Published online: 12 January 2026

exploration of alternative hardware architectures beyond conventional complementary metal oxide semiconductor (CMOS) technology. Among the emerging candidates, large-scale memristor arrays have attracted significant attention due to their potential for high density, fast switching speeds, multilevel conductance, and low power consumption, making them highly promising for next-generation data storage and computing systems. However, the limited energy efficiency, complex fabrication processes, and computational constraints inherent to transition-metal oxide and organic-molecule-based memristors continue to pose major challenges to their widespread adoption and practical implementation [8].

Recent advancements in neuromorphic systems (NSs) utilizing memristive synapses have shown promising results in applications such as perceptron [9, 10], reinforcement learning, and networks for long and short-term memory processing [11, 12]. However, formal neuromorphic systems (FNSs) trained via gradient descent optimization algorithms face significant challenges, including complex hardware configurations due to device stability issues and cycle-to-cycle (C2C) fluctuations [13]. To address these issues, alternative approaches like reservoir computing (RC) have been proposed, offering potential solutions to these challenges [12, 14].

reservoir computing (RC) systems are composed of two main elements: a reservoir and a readout layer. The reservoir, a dynamic system with short-term memory, performs nonlinear processing on input signals to extract key features. The readout layer generally implemented as a simple linear network analyzes the extracted spatiotemporal features. The efficiency of this architecture arises from the fact that only the readout layer requires training, thereby substantially reducing the overall computational cost and training complexity [15]. Various studies have successfully implemented RC systems using atomic switch networks, photonic systems and memristive devices, demonstrating their potential for high efficiency. However, training the readout layer still relies on power-intensive gradient descent algorithms, whether implemented in software or hardware [16–21].

Researchers have explored a variety of transition-metal dichalcogenides (TMDs), including WS_2, $MoSe_2$, $HfSe_2$, and MoS_2, for crossbar memristor fabrication. However, conventional approaches such as mechanical exfoliation and sputtering often result in non-uniform thickness, morphological inconsistencies, and limited scalability, leading to performance variability [22, 23].Transition-metal oxide memristors, while widely investigated, still face challenges related to energy efficiency, fabrication complexity, and limited computational performance, thereby motivating the search for advanced material systems [24–27]. Organic memristors offer advantages of flexibility and low-cost processing, yet their device and array level stability remains a major bottleneck for long-term reliability [28, 29]. Halide perovskite devices exhibit fast switching and rich ionic dynamics, but suffer from ion migration and environmental sensitivity, restricting their durability and integration potential [30, 31]. Likewise, 2D-material memristors enable ultrathin scaling and heterogeneous integration but continue to face challenges in achieving uniformity and high endurance at wafer scale [32, 33]. By contrast, nanocomposite memristors such as CeO_2-based vertically aligned nanostructures, composite-interface oxides, and polymer oxide hybrids consistently demonstrate low operating voltages, large ON/OFF ratios, excellent endurance, and stable multi-level resistive states. Their inherent compatibility with crossbar architecture makes them highly suited for neuromorphic and reservoir computing applications [34]. Notably, memristor crossbar arrays have already achieved high recognition accuracy on benchmark datasets (e.g., MNIST), while operating at synaptic energy levels in the picojoule to femtojoule range, underscoring their efficiency for edge intelligence [35]. Collectively, these advances highlight nanocomposites as a scalable, stable, and energy-efficient materials platform for next-generation neuromorphic hardware.

In the present study we proposed a hybrid nanocomposite device Ag/$Fe_{50}W_{50}$/Pt with dynamic characteristics to construct an RC for multitasking pattern classifications. The cross-bar array robust memristor structure based on hybrid nanocomposite, which shows reproducible bipolar memristor switching with endurance up to 10^7 having ultralow set and reset voltage. The polymorphic nature of the material likely contributes to the vertically aligned grain boundaries (GBs) structure, which creates restricted diffusion pathways. During resistive switching (RS), Ag ions preferentially migrated along these aligned GBs, facilitating the formation of stable conduction paths and enabling reliable RS behavior. Fabricated memristor crossbar arrays based on these films exhibited dependable RS with stable multilevel resistance and minimal cyclic variation (<8.7%), high device yields (>85.7%), and extended retention times (>10^6s). The neuromorphic device exhibiting excellent electrical-responsive behavior and memory capabilities, enabling memorization, and pre-processing of electrical inputs. This research presents a material-algorithm co-design strategy to develop efficient and cost-effective neuromorphic systems capable of multi-task learning. The system achieved 87.82% accuracy in simultaneous multi-task classification and 99.25% accuracy in gesture recognition using spatiotemporal dynamics, demonstrating its strong potential for versatile, high-performance neuromorphic computing.

2 Experimental

The synthesis of $Fe_{50}W_{50}$ nanocomposites by using precise quantities of Fe_3O_4 and WS_2 nanoparticles precursors. The synthesis of $Fe_{(1-x)}W_{(x)}$, hybrid nanocomposite nanoparticles involved ethylene glycol, followed by the addition of precursors and stirring at room temperature. The mixture was initially heated at 80 °C for one hour to initiate the reaction, followed by a slight increase in temperature that led to gelation after approximately two hours. Finally, the temperature was raised to 200–300 °C to complete the combustion process. The resulting samples, denoted as $Fe_{(1-x)}W_{(x)}$, contained equal weight percentages of nanoparticles, for example, $Fe_{50}W_{50}$ comprised 50 wt% magnetite Fe_3O_4 and 50 wt% WS_2 nanoparticles.

The newly developed 10 × 10 crossbar array memristor used in this work features a simple Ag/$Fe_{50}W_{50}$/Pt structure. The bottom electrode pattern, 4 µm wide, was created using lithography process. A 3 nm layer of Ti and 17 nm of Pt were then deposited via DC sputtering, followed by photoresist removal through a lift-off process. After the bottom electrode the second lithography step was done and switching layer of thickness 40 nm was deposited by using a thermal evaporator followed by the lift off process. In the third step the top electrode was patterned by lithography process, and 120 nm of Ag was deposited by thermal evaporation followed by the lift off process. All the stages of the 10 × 10 crossbar array memristor device fabrication with optical images is shown in Supplementary Figure S1.

3 Results and discussion

Figure 1(a) presents a schematic of the crossbar array structure fabrication, achieved through optimized deposition of the bottom electrode, switching layer, and top electrode, followed by a lift-off process. Figure 1(b) displays an optical image of a typical 10 × 10 $Fe_{50}W_{50}$ hybrid nanocomposite (HNM) crossbar array device. Figures 1c shows the schematic diagram of array bar structure and crystal structure of $Fe_{50}W_{50}$ hybrid nanocomposite. Figure 1d shows the cross-section high angle annular dark-field (HAADF) confirms the thickness of the bottom and switching layer. The Fig. 1e shows scanning transmission electron microscopy (STEM) elemental overlap mapping, along with their corresponding individual elemental distributions of silver (Ag), iron (Fe), tungsten (W), oxygen (O), sulfur (S), and platinum (Pt) respectively.

In the Fig. 2(a) shows the I-V switching cycles of the Ag/$Fe_{50}W_{50}$/Pt cross bar array memristor device were performed by applying voltage sweeps (−0.8 V to 0.8 V) to the Ag top electrode while grounding the Pt bottom electrode. The device exhibited stable, electroforming-free switching behavior over multiple cycles, with consistent performance and minimal variability.

During the positive sweep, a sharp current increase at 0.18 V indicated the set process, transitioning the device from HRS to LRS. The memristor exhibited ultra-low and uniform set and reset voltages. Under negative bias, the device

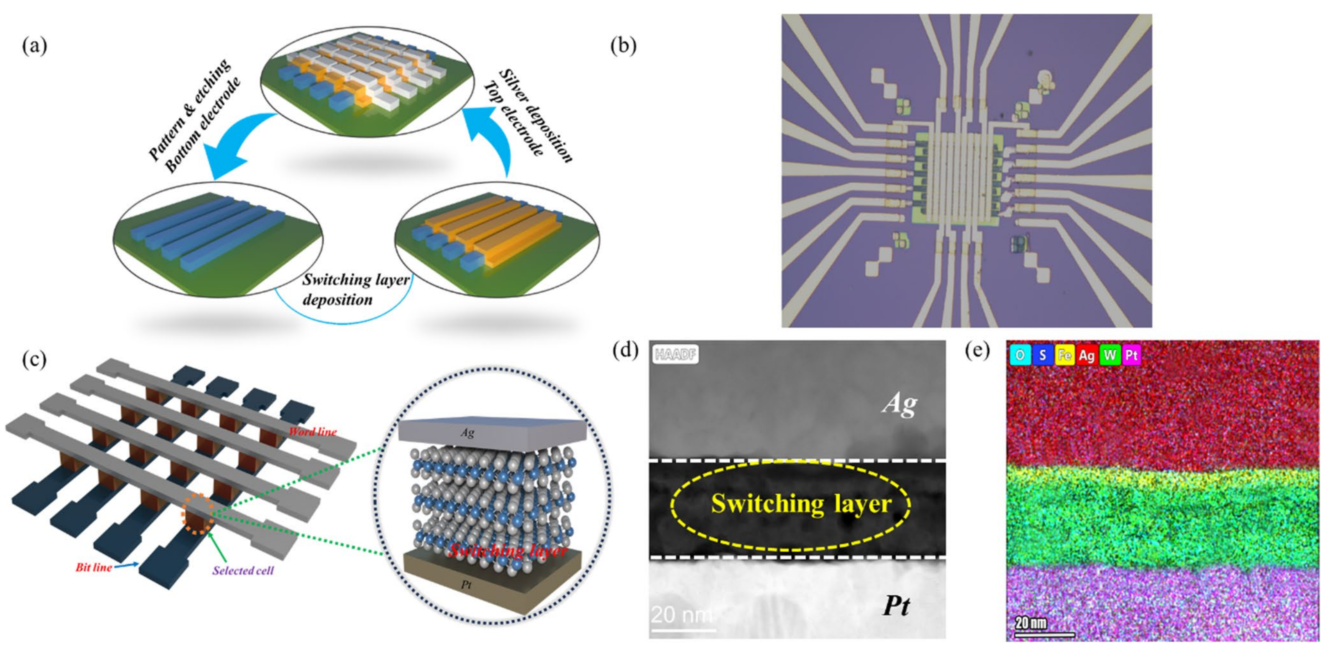

Fig. 1 (**a**) Schematic of fabrication process for10 × 10 memristor cross-bar array. The bottom Pt electrode, patterned by using lithography process after that $Fe_{50}W_{50}$ (HNM) deposited as switching layer. The top Ag electrode assembly is subsequently patterned using lithography process same as bottom electrode. (**b**) Optical image of the $Fe_{50}W_{50}$ (HNM) 10 × 10 memristor cross-bar array. (**c**) Schematic diagram of the artificial array bar synapse having projection of the material structure as a switching layer. Cross-section HRTEM image of a $Fe_{50}W_{50}$ (HNM) device. (**e**) STEM-Eds mapping for elemental analysis of HNM

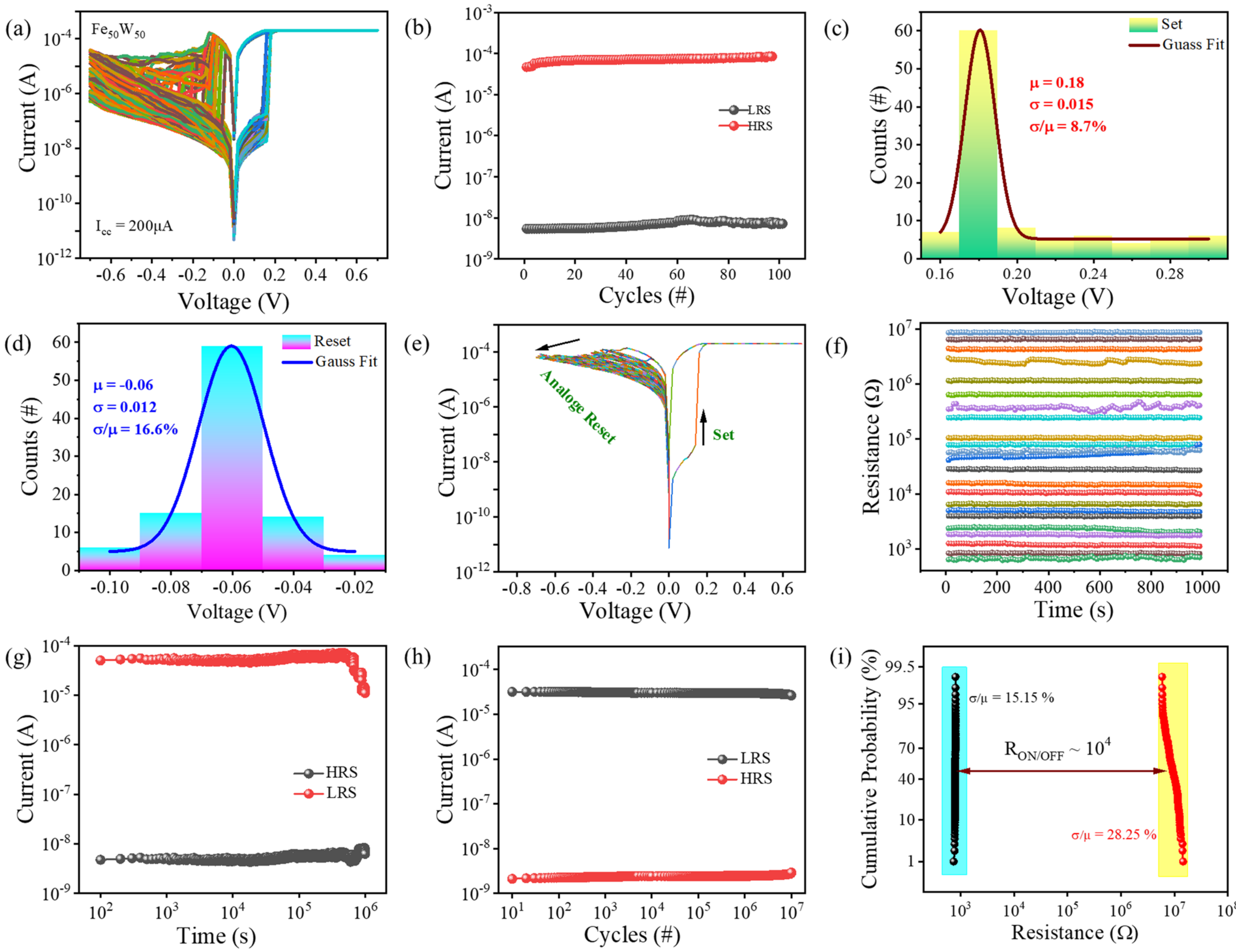

Fig. 2 (**a**) 100 switching cycles of a single $Fe_{50}W_{50}$ hybrid nanocomposite (HNM) array-bar memristor, demonstrating stable and repeatable resistive switching behavior. (**b**) Endurance stability of the switching cycles. (**c**) Set distribution histogram of the switching cycles. (**d**) Reset distribution histogram of the switching cycles. (**e**) The digital set and analog reset current–voltage (I–V) characteristics were examined by gradually increasing the reset voltage from – 0.3 V to – 0.7 V in increments of 0.01 V. (**f**) Retention measurements were conducted for multiple resistance states over a duration of 10^3 seconds. (**g**) Retention stability of the $Fe_{50}W_{50}$ (HNM) array bar device up to 10^6 cycles. (**h**) Endurance stability of the $Fe_{50}W_{50}$ (HNM) array bar device up to 10^7 cycles. (**i**) Cumulative probability distribution of the switching cycles for the $Fe_{50}W_{50}$ hybrid nanocomposite device

exhibited stable low resistance state (LRS) until − 0.06 V, triggering a transition to a high resistance state (HRS), indicative of a reset process. Endurance tests and statistical analyses in Fig. 2 (b-d) revealed consistent switching behavior with low variation in set (16.6%) and reset (8.7%) parameters, suggesting improved uniformity. Gradual resistance modulation for neuromorphic applications was achieved by incrementally increasing the reset-stop voltage by 0.01 V during I-V characterization as shown in Fig. 2(e), enabling fine control of synaptic weights. Subsequent I-V sweeps and retention tests in Fig. 2(f) demonstrated stable retention of multiple high-resistance states for over 10^3 seconds each, indicating robust synaptic emulation. Overall device performance in Fig. 2(g, h) showed excellent retention (> 10^6 seconds) and endurance (> 10^7 cycles). This memristive behavior is attributed to heterogeneous grain boundaries with lattice disorders, potentially hosting unique interface states compared to homophase boundaries. These boundaries are hypothesized to facilitate conductive filament formation via electrochemical metallization (ECM) driven by Ag ion diffusion through the $Fe_{50}W_{50}$ nanocomposite. Unlike vacancy-controlled memristors (VCM) that utilize sulfur vacancies, our devices operate as ECM memristors, where metal ion deposition occurs via electrochemical reactions [36, 37].

To mitigate sneak-path currents in passive-circuit crossbar arrays, achieving a high Ion/Ioff ratio in memristors is crucial. A higher Ion/I_{off} ratio reduces sneak-path currents effectively as well as enables larger passive circuits. The $Fe_{50}W_{50}$ hybrid nanocomposite crossbar array demonstrates forming free and extremely small set/reset voltages and higher $R_{ON/OFF}$ (10^4). To validate the operational capability of the array bar device, we conducted various I-V characteristic measurements on array cells. The results demonstrated excellent switching cycles across the cells, with no signs of degradation in HRS, as shown in the Supplementary Figure (S2). Cycle-to-cycle variations at room temperature were evaluated using cumulative probability, as illustrated in Fig. 2(i). The increased high resistance state value (HRS) reflects the very low leakage current in $Fe_{50}W_{50}$ hybrid nanocomposite crossbar array device. By down scaling the device size 100 × 25 µm also reduces the conduction paths indicating that the leakage current of devices decreased [38]. To assess the reproducibility of the device, we evaluated 25 array bar units, and the variations in the set and reset cycles are illustrated in the Supplementary Figure S3(a, b). These characteristics make promising candidates for addressing the sneak-path problem in memristor-based crossbar arrays. Furthermore, the device shows excellent environmental stability and no degradation in the switching cycles after 6 months shown in Supplementary Figure (S4). The array bar structure exhibits substantial advantages over previously reported synapses, as summarized in Supplementary Table T1.

Figure 3a depicts a schematic of a biological synapse, with the memristor's top and bottom electrodes representing pre- and postsynaptic terminals. Synaptic plasticity is analogous to the memristor's in-memory computing capability. Figure 3(b) demonstrates five cycles of long-term potentiation (LTP) and depression (LTD) behaviors in response to ± 0.44 V, 1µs programming pulse. The memristor's conductance exhibits gradual changes in response to varying stimulus pulse characteristics (interval, amplitude, width, and number), mimicking synaptic plasticity. The linearity of synaptic weight changes during long-term potentiation (LTP) and long-term depression (LTD) serves as a key performance indicator for electronic synapses, reflecting their functional efficacy in neuromorphic systems as shown in Supplementary Figure (S5). Furthermore the Ag/$Fe_{50}W_{50}$/Pt memristor demonstrates paired-pulse facilitation (PPF), a crucial synaptic function observed in biological synapses [39]. When two presynaptic spikes (0.6 V, 1 µs) are delivered consecutively to the top electrode with a 1 µs interval, the second spike elicits an excitatory postsynaptic current (EPSC) greater than the first. This behavior mimics short-term plasticity (STP) in biological synapses, where synaptic strength changes over microseconds to milliseconds. The PPF index, which represents the ratio

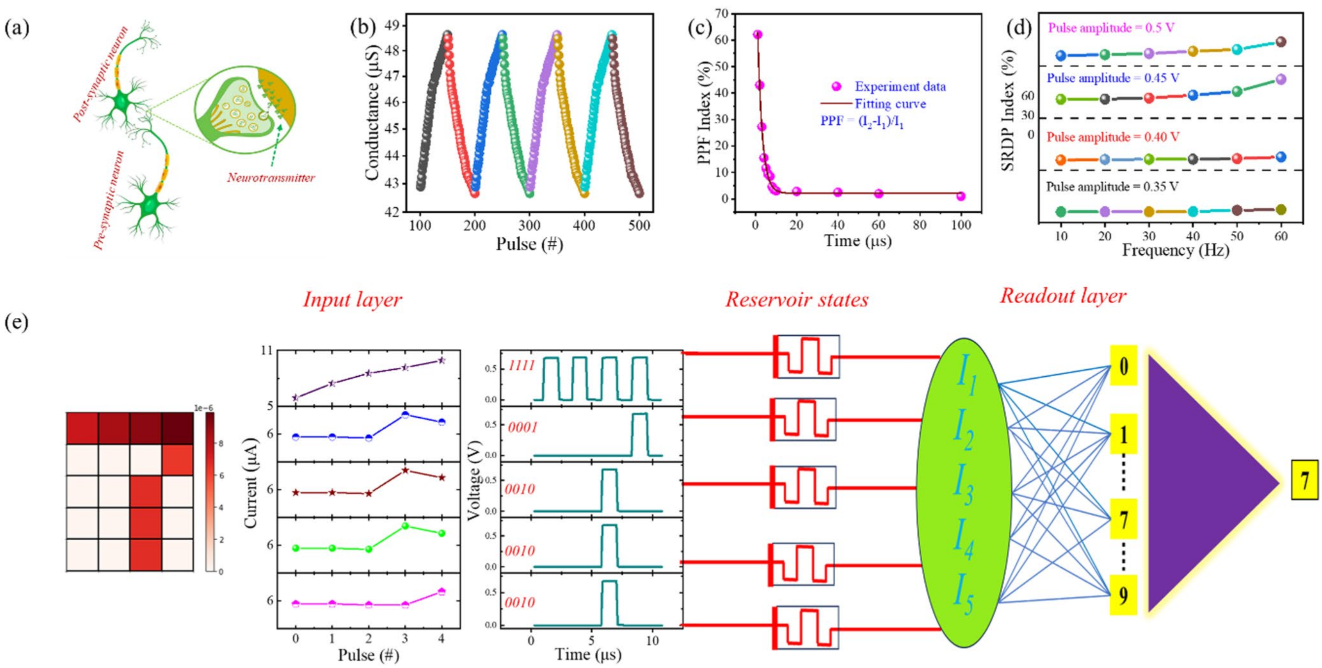

Fig. 3 (**a**) Biological synapse of synaptic system (**b**) Multiple cycles of potentiation and depression induced by electrical pulses with an amplitude of 0.44 V. (**c**) PPF (%) of the $Fe_{50}W_{50}$ hybrid nanocomposite. (**d**) Change in EPSC depending on the pre-synaptic pulse frequencies from 10 H to 60 Hz where $Gain_{max}$ depends on the pulse amplitude (0.35,0.40,0.45,0.50). (**e**) Schematic representation of the Ag/$Fe_{50}W_{50}$/Pt memristive RC circuit. Demonstration of the system's capability to process image data, specifically the conversion of the digit "7" from a 5×4 pixel representation. The output currents of the memristor are measured under five distinct pulse trains, each designed to represent the pixel states of "1111", "0001", "0010", "0010", and "0010". The experimental setup for the reservoir computing system is illustrated, including the input pulse scheme, the resulting encoded reservoir state, and the readout layer

of the second EPSC to the first, decreases as the interval between pulses increases, as shown in Fig. 3(c). This phenomenon reflects how learning and memory decay over time and demonstrates the memristor's ability to emulate key aspects of biological synaptic behavior, including facilitation and depression in response to closely timed stimuli. The PPF index can be calculated by using this expression [40].

$$PPF = (I_2 - I_1)/I_1 \times 100 \quad (1)$$

where I_1 and I_2 represent the first and second peak amplitudes, respectively. The PPF index decreases as the pulse interval (Δt) increases, demonstrating short-term plasticity [41]. The highest PPF value (approximately 65%) occurs at the shortest interval (Δt = 1µs), while the lowest PPF (about 0.3%) is observed at the longest interval (Δt = 0.01ms). This behavior, along with its exceptional repeatability, confirms the memristor's ability to mimic biological synaptic short-term memory characteristics, potentially contributing to the development of efficient neuromorphic computing systems. Spike-Timing-Dependent Plasticity (STDP) is a biological learning mechanism observed in the brain that adjusts the strength of connections between neurons, known as synapses, based on the precise timing of spikes (action potentials) between them [42, 43]. To demonstrate STDP behavior in our Ag/$Fe_{50}W_{50}$/Pt device, we applied carefully designed pulse stimuli to the pre-synaptic and post-synaptic terminals. Supplementary Figure S6 (a) illustrates the schematic representation of the stimulating pulses, which consist of two overlapping spikes. The pre-synaptic and post-synaptic stimulations were implemented using the pulse of magnitudes 0.5 V to effectively modulate the device's conductance and emulate synaptic plasticity as shown in Supplementary Figure S6 (b).

Short-term synaptic behavior function as dynamic filters, where changes in synaptic weight or excitatory post-synaptic current (EPSC) are influenced by spike frequency [44, 45]. In memristors, the post-synaptic current can increase with changes in voltage due to the modulation of the device's conductance. When a voltage is applied across a memristor, it can alter the distribution of ions or vacancies within the device, which in turn changes its resistance. For instance, in memristive devices like those based on transition-metal oxides, applying a voltage can cause a shift in the internal ionic configuration, leading to a change in conductance and thus affecting the post-synaptic current [44, 46]. This change in conductance is akin to adjusting synaptic weights in biological systems, where higher conductance corresponds to a stronger synaptic connection, resulting in increased post-synaptic current. Additionally, the ability to control this change in conductance through precise voltage adjustments allows for the emulation of synaptic plasticity, which is crucial for neuromorphic computing applications as shown in Fig. 3(d). As the voltage increases the membrane potential is closer to the threshold for activating voltage-gated ion channels, such as calcium channels. These channels are critical for initiating the biochemical processes that lead to synaptic potentiation. The maximum EPSC response is observed at 0.5V at 60 Hz because both voltage and frequency are high, that leads to a substantial change in synaptic potentiation strength.

The device exhibits short-term plasticity (STP), indicated by transient currents in response to diverse inputs [47]. An RC system, utilizing the memristor's non-volatile memory, consists of input, reservoir, and readout layers [48]. Transient currents, elicited by input pulse sequences, function as reservoir states and are subsequently analyzed during the readout phase. For example, the digit "7" is encoded by five pixel patterns corresponding to the temporal pulse sequences "1111," "0001", "0010," "0010," and "0010" as shown in Fig. 3(e). These sequences involve a 0.8 V, 0.5 µs potentiation pulse followed by a 0.1 V read voltage. The resulting output current variations are dependent on the input patterns. The significant current differentiation between the "1" and "0" states across the pulse sequences confirms the memristor's suitability for reservoir computing systems.

Reservoir computing (RC) systems are gaining attention for their ability to process temporal information with reduced training costs and computational resources. The reservoir and readout networks of these systems are implemented on synaptic devices, which exhibit both volatile and non-volatile memory properties. Memristors based on vacancy diffusion and oxygen ions, with inherent short-term memory, are essential for implementing reliable and scalable hardware-based readout networks in reservoir computing systems [49, 50]. Thus, achieving a consistent non-volatile memristive response with high switching speed is crucial for developing an energy-efficient reservoir computing system. 5(a) displays 16 distinct reservoir states, each clearly separated to uniquely represent different pixel combinations. When we apply the pulse "1" responds to the increase in the current, while "0" responds to decrease in current. The non-volatile nature of V_O generated during a 0.8 V, 0.5 µs pulse interval causes changes in the memristor's conductance, resulting in temporal output currents that encode information about multitasking recognitions. These states served as the reservoir output for training and testing the readout network.

4 Multitasking recognitions

Figure4a presents the schematic of RC system showing multi-task recognition ability, which closely resembles the architecture of the human brain in terms of in-memory configuration. This includes the ability to learn and differentiate between various attributes of a given object, such as the type and size of specific items (e.g., different garments). Initially, images of garments are processed by the $Fe_{50}W_{50}$ hybrid nanocomposite electronic reservoir, which employs its intrinsic fading memory to generate semantic features.

These features are then fed into the hybrid nanocomposite diode readout map for garment classification. The reservoir and readout maps are utilized for garment dimension classification, employing alphanumeric symbols (“L”,“M “S,“) for pullovers and numerals for sandals. This demonstrates the system’s versatility in multi-task learning, applying the same computational architecture to different aspects of garment recognition. Figure 4b schematically depicts the circuit of the $Fe_{50}W_{50}$ hybrid memristor reservoir. The $Fe_{50}W_{50}$ hybrid memristor receives various electrical signals, generating a range of distinct currents. The signal processing chain involves converting currents to voltages via trans-impedance amplifiers, followed by digitization using analog-to-digital converters (ADCs). These digital signals undergo post-processing before being converted back to analog form by digital-to-analog converters (DACs). This architecture efficiently integrates analog and digital processing for neuromorphic computation. The readout layer utilizes a memristor array, with each cell containing a single memristor as an adjustable weight. Figure 4(c) illustrates the data sources garment images are obtained from Fashion-MNIST, and their corresponding dimensions are represented by letter and digit images from E-MNIST and MNIST datasets [51–53]. All optical images are standardized to 28 × 28 pixels for consistency and computational efficiency. The image processing pipeline begins with binarization and trimming of edge pixels as shown in Fig. 4 (d). The remaining pixels are reorganized into 140 × 5 optical sequences and serve as input to a dynamic reservoir of 140 $Fe_{50}W_{50}$ nanocomposite-based visual neurons. This electrical reservoir, mimicking and primary visual cortex functions, transforms input sequences into 140-long visual features as electric currents.

The device exhibits digital-to-analog behavior at the cellular level, allowing for the direct input of electrical stimuli

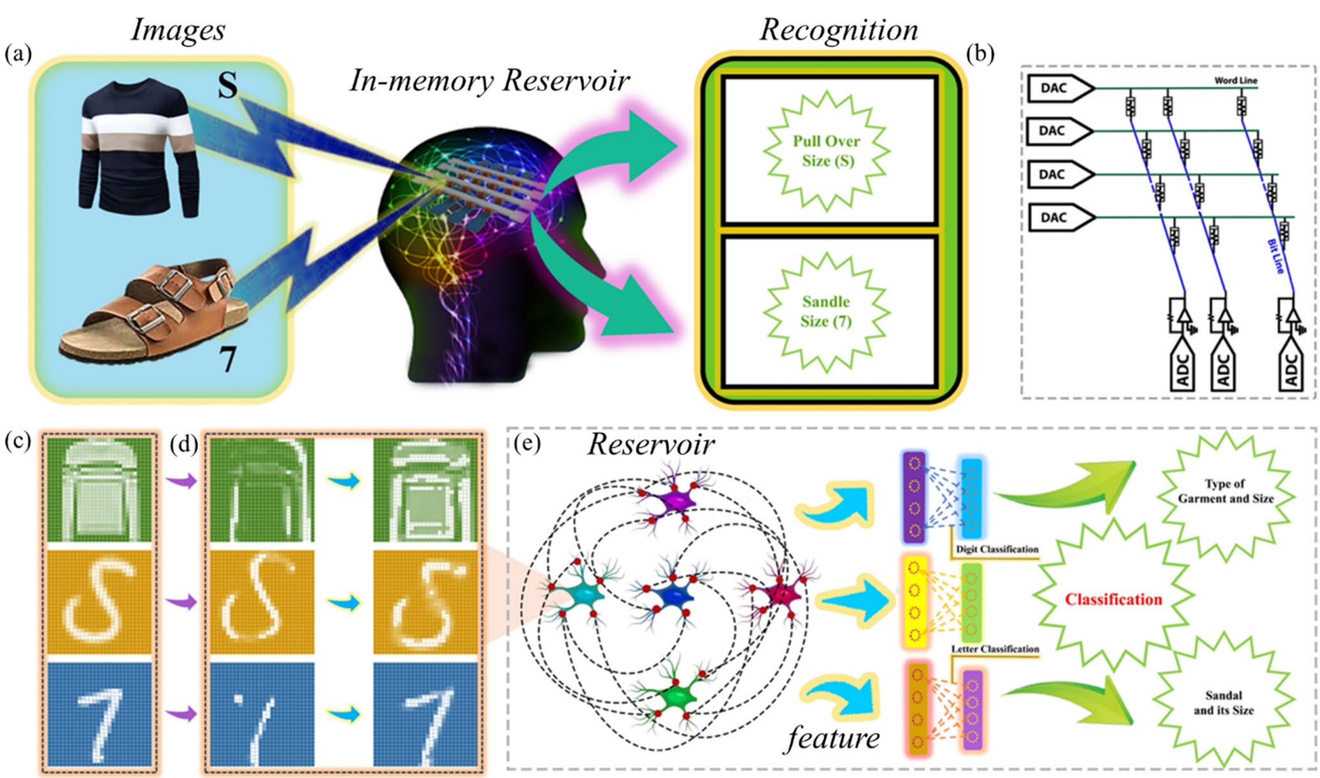

Fig. 4 (**a**) Framework for simultaneous recognition of multiple tasks using a reservoir computing paradigm. A $Fe_{50}W_{50}$ (HNM) array bar device reservoir receives garment images with corresponding size information. Memristive readout maps classify these inputs. (**b**) The readout layer is implemented by an ionic diode crossbar circuit. (**c**, **d**) Input data comprises garment images and size labels sampled from FMNIST, E-MNIST, and MNIST datasets, which undergo software pre-processing before being fed to the reservoir. (**e**) The $Fe_{50}W_{50}$ (HNM) array bar enables autonomous, training-free discriminative feature extraction across multiple tasks through its task-adaptive memristive diode readout, intrinsic fading memory, and integrated multi-task classification framework

representing various images or tasks into the RC system. The reservoir computing architecture comprises untrained delayed feedback dynamic nodes, implemented using $Fe_{50}W_{50}$ hybrid nanocomposite memristors as shown in (Fig. 4e, cherry nodes). The learning process exclusively optimizes the readout map connections, which link reservoir neurons to output neurons (Fig. 4e, arrows connecting to purple, yellow, and orange nodes). This approach leverages the intrinsic dynamics of the reservoir while focusing training efforts on the readout layer, enhancing computational efficiency. The electrical reservoir computing (RC) system, leveraging the fading memory of a hybrid nanocomposite, demonstrates significant advantages over conventional neural networks. It achieves reduced data processing costs and accurately emulates fast processing functionality. A series of comprehensive testing of this multi-task electrical RC system revealed its efficacy in various cognitive tasks, showcasing the potential of this approach for efficient neuromorphic computing applications. This process relies on the fading memory dynamics of $Fe_{50}W_{50}$ hybrid nanocomposite. The extracted image feature undergoes processing through a hybrid nanocomposite readout map, functionally analogous to the striate cortex in biological visual recognition systems. The RC system, with specific accuracies of 98.79% for letters, 87.82% for digits, and 91.51% for garments, after 100 epochs demonstrate effective multi-task learning capabilities. As the number of epochs increases, the accuracy improves while the entropy loss decreases as shown in Supplementary Figure S7 (a-f). Notably, the majority of individual classes in this hybrid system achieve accuracy rates exceeding 85%, demonstrating its effectiveness in multi-task classification scenarios.

Figure 5b presents a comparative analysis of the electrical reservoir computing system against single and double-layered artificial neural networks (ANNs). The reservoir system achieves 87.825% accuracy, comparable to single-layered (89.65%) and double-layered (89.75%) ANNs. Notably, the reservoir system demonstrates superior weight efficiency, utilizing only 1.4k weights compared to 5.5k and 315k in single- and double-layered ANNs, respectively. This highlights the system's computational efficiency while maintaining competitive performance. The device demonstrates superior performance in terms of energy consumption, accuracy, and scalability compared to previously reported memristor devices, as summarized in Supplementary Table (T2). When evaluated in terms of accuracy per weight, the reservoir computing (RC) system exhibits fourfold higher efficiency (0.062) compared to the single-layer ANN (0.016) and is approximately 200 times more efficient than the double-layer ANN (0.00028), highlighting its superior computational utilization and learning efficiency. Figure 5c presents a three-dimensional visualization of high-dimensional feature vectors encoded by the reservoir, using linear discriminative analysis (LDA). Each data point represents a sample, with color indicating garment class and point size reflecting class frequency. The visualization demonstrates effective class

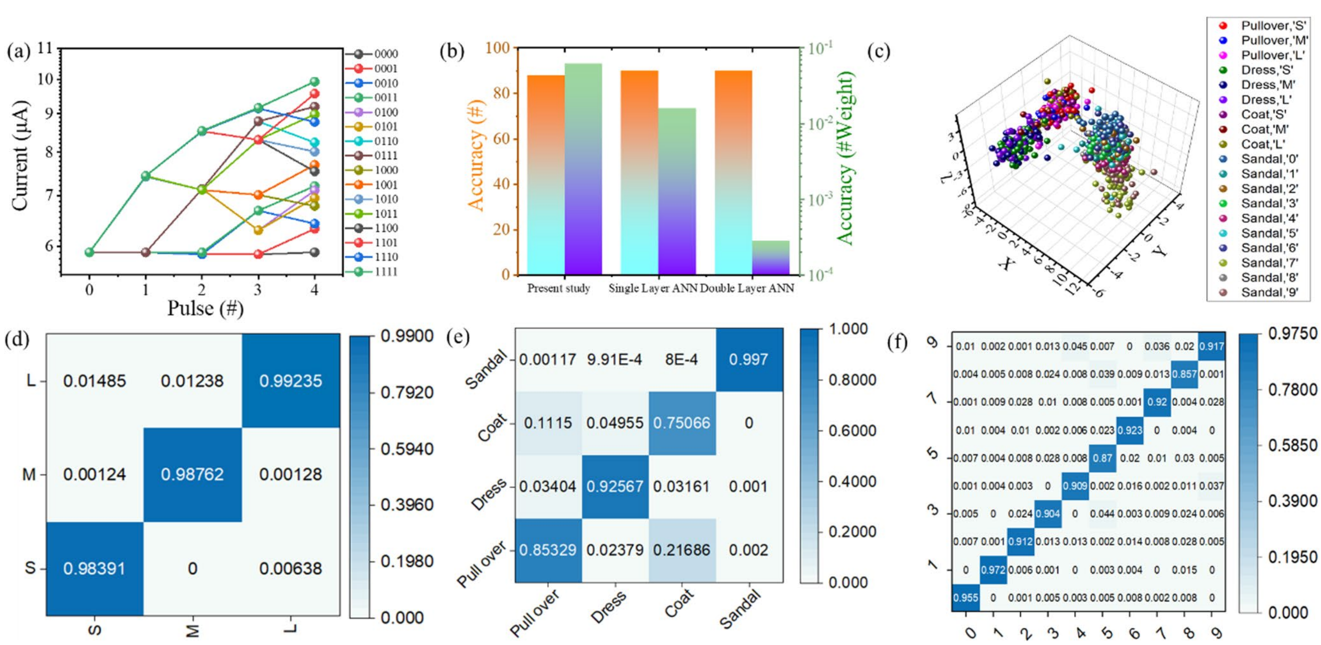

Fig. 5 (**a**) Experimental current responses to 4-bit electrical pulse trains (0000) to (1111). (**b**) Accuracy versus trainable weights: electrical reservoir computing, single-layer ANN, and double-layer ANN. (**c**) Three-dimensional visualization of the feature vector distribution was carried out using linear discriminant analysis (LDA). (**d-e**) Confusion matrices of the reservoir computing system for three sub-tasks, demonstrating high accuracy with dominant diagonal elements

separation and intra-class clustering, indicative of the reservoir's robust feature extraction capabilities. In the Fig. 5(d-f) presents independent confusion matrices for each dataset. The system achieves accuracy of 91.51% for MNIST, 98.79% for EMNIST-letters, and 87.825% for FMNIST. The predominance of diagonal elements in these matrices indicates high class-wise accuracy for each sub-task.

The electrical reservoir computing (RC) system demonstrates remarkable capabilities in processing not only two-dimensional images but also dynamic video data, particularly those attained by dynamic vision sensors (DVS) [54]. This study focuses on gesture recognition performance on a subset of the DVS128 Gesture dataset, focusing on four distinct dynamic hand movements: arm roll, hand clapping, air drums and waving, and air guitar.

The system's functionality is illustrated through an example of a hand clapping waving gesture. The event video underwent spatial down sampling to a resolution of 28×28 pixels and temporal binning into 32 discrete frames. To create the dataset, five frames were extracted at equal intervals. The $Fe_{50}W_{50}$ hybrid nanocomposite array RC system compresses 3D event streams into 2D features, which are processed by a non-volatile readout layer, with integer-denoted interconnections for efficient gesture classification. The pseudo-inverse method is used to optimize the readout layer for real-time edge learning. The enhanced readout map interprets the reservoir feature map, producing an analog current-based classification vector. This vector is then digitized to predict gesture types from the event stream, as depicted in Fig. 6(a). Principal component analysis (PCA) visualization of reservoir feature maps of test and train data effectively demonstrates clustering of same-class samples and clear separation between different gesture classes as shown in Fig. 6(b). Figure 6(c) presents a confusion matrix with strong diagonal elements, indicating high class-wise classification accuracy for each gesture type. The system correctly identifies the hand clapping, air drums air rolls and air guitar gestures. The system achieves 98.62% overall accuracy in recognizing all gestures as shown in Fig. 6(d). As the epoch number during the training process increases, the classification accuracy improves while the cross-entropy loss decreases, as shown in Fig. 6(e). This innovative approach demonstrates the potential of RC systems for efficient video feature extraction and classification.

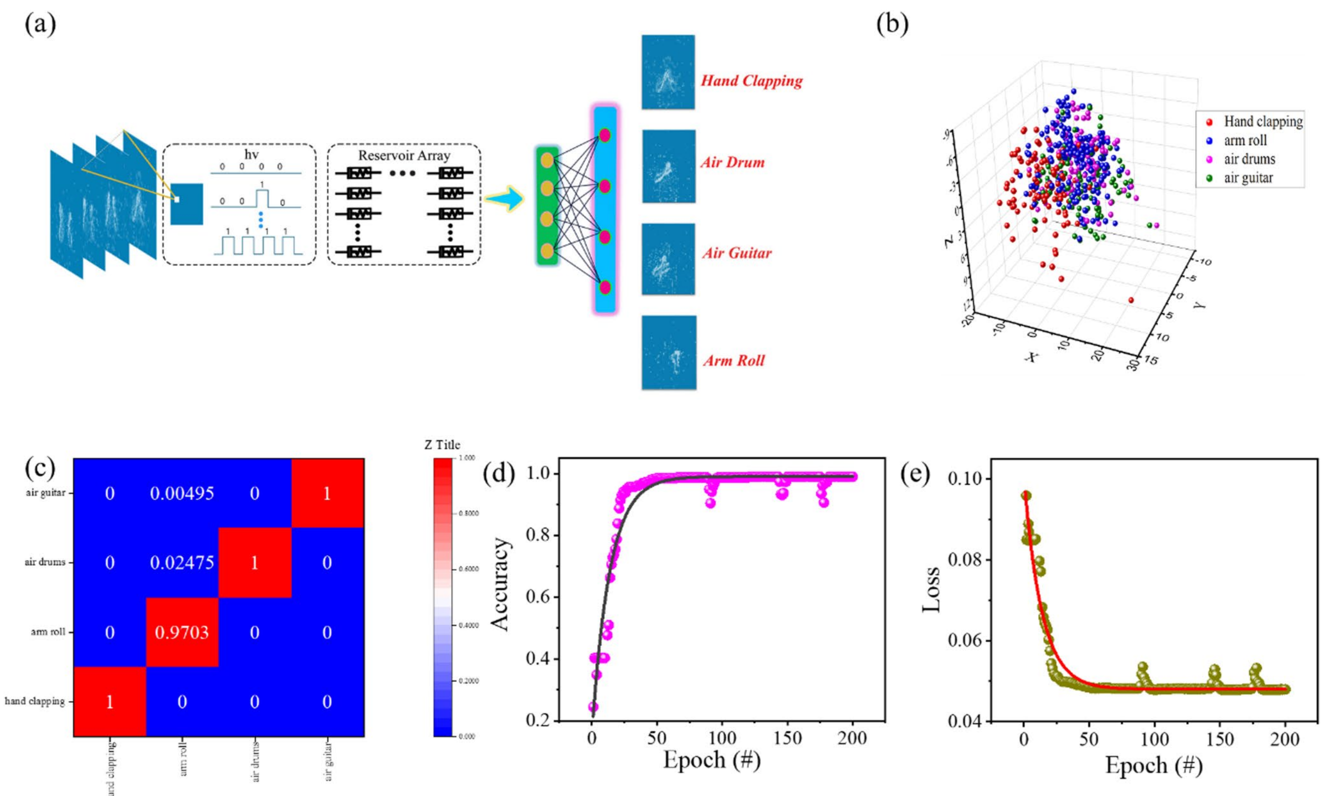

Fig. 6 (**a**) A schematic illustration of the event stream frames as processed by the reservoir computing (RC) system. The event video was spatially down-sampled to 28×28 pixels and temporally binned into 32 frames. (**b**) Principal Component Analysis (PCA) of the reservoir system's feature map reveals linearly separable clusters corresponding to different gestures in a 2D-dimensional projection. (**c**) The confusion matrix exhibits a strong diagonal dominance, indicating high classification accuracy across gesture classes. (**d-e**) Training curves illustrate the progression of classification accuracy and loss over 200 in situ training epochs

5 Conclusion

In this study, we successfully developed a highly reliable artificial electronic synaptic device in a large-scale 10×10 crossbar array structure. The hybrid nanocomposite material (HNM) arrays demonstrated the formation of aligned grain boundaries (GBs), showcasing their potential for large scale artificial synapse applications. The array architecture incorporated preferential diffusion paths along uniformly aligned GBs, resulting in superior spatial and temporal uniformity. The fabricated crossbar structure exhibited excellent performance characteristics, including long retention, good endurance, low power consumption, and linear conductance updates. The memristor-based dynamic reservoir computing (RC) system demonstrates excellent performance due to its electrical response, fading memory, and echo state property. The electrical RC achieves high accuracies in various recognition tasks handwritten character recognition (98.79%), garment classification (88.92%) and digit classification (91.51%). A hybrid nanocomposite-based reservoir computing (RC) system achieved a high overall accuracy of 87.82% in simultaneous garment attribute recognition, demonstrating superior performance among similar systems. This RC approach exhibits significantly reduced training costs compared to artificial neural networks (ANNs), rendering it suitable for edge computing. Furthermore, the system attained 98.62% accuracy in gesture classification, addressing limitations of conventional sensing-computing paradigms. This research showcases a promising material-algorithm co-design strategy for efficient neuromorphic systems, emphasizing robust and cost-effective multi-task learning capabilities within an RC framework.

Supplementary Information The online version contains supplementary material available at https://doi.org/10.1007/s42114-025-01566-w.

Acknowledgements This research is supported by the National Research Foundation (NRF) of Korea, funded by the Ministry of Science and ICT (RS-2024-00468995, RS-2025-02303505).

Author contributions Author Credit Statement: Faisal Ghafoor: Writing original draft preparation, Data curation, material synthesis, Visualization, Formal analysis. Honggyun Kim: Methodology, Investigation, Formal analysis. Hui Zhang: Simulation, Visualization. Bilal Ghafoor: Investigation, data curation, software Myungjae Lee: Data curation, Investigation. Methodology and Investigation. Tuo Shi: Software, Visualization Deok-kee Kim: Conceptualization, Writing – review & editing, Supervision.

Funding This research is supported by the National Research Foundation (NRF) of Korea, funded by the Ministry of Science and ICT (RS-2024-00468995, RS-2025-02303505).

Data availability The datasets generated during and/or analyzed during the current study are available from the corresponding author on reasonable request.

Declarations

Competing interests The authors declare no competing interests.

References

1. Seo S et al (2021) An optogenetics-inspired flexible Van der Waals optoelectronic synapse and its application to a convolutional neural network. Adv Mater 33(40):2102980
2. Boybat I et al (2018) Neuromorphic computing with multi-memristive synapses. Nat Commun 9(1):2514
3. Yao P et al (2020) Fully hardware-implemented memristor convolutional neural network. Nature 577(7792):641–646
4. Xia Q, Yang JJ (2019) Memristive crossbar arrays for brain-inspired computing. Nat Mater 18(4):309–323
5. Kumar S, Williams RS, Wang Z (2020) Third-order nanocircuit elements for neuromorphic engineering. Nature 585(7826):518–523
6. Sun K, Chen J, Yan X (2021) The future of memristors: materials engineering and neural networks. Adv Funct Mater 31(8):2006773
7. Zhang Y et al (2020) Brain-inspired computing with memristors: challenges in devices, circuits, and systems. Appl Phys Rev. https://doi.org/10.1063/1.5124027
8. Lanza M et al (2022) Memristive technologies for data storage, computation, encryption, and radio-frequency communication. Science 376(6597):eabj9979
9. Prezioso M et al (2015) Training and operation of an integrated neuromorphic network based on metal-oxide memristors. Nature 521(7550):61–64
10. Emelyanov A et al (2016) First steps towards the realization of a double layer perceptron based on organic memristive devices. AIP Adv. https://doi.org/10.1063/1.4966257
11. Li C et al (2019) Long short-term memory networks in memristor crossbar arrays. Nat Mach Intell 1(1):49–57
12. Wan W et al (2022) A compute-in-memory chip based on resistive random-access memory. Nature 608(7923):504–512
13. Wang Z et al (2020) Resistive switching materials for information processing. Nat Reviews Mater 5(3):173–195
14. Prezioso M et al (2018) Spike-timing-dependent plasticity learning of coincidence detection with passively integrated memristive circuits. Nat Commun 9(1):5311
15. Tanaka G et al (2019) Recent advances in physical reservoir computing: A review. Neural Netw 115:100–123
16. Du C et al (2017) Reservoir computing using dynamic memristors for temporal information processing. Nat Commun 8(1):2204
17. Midya R et al (2019) Reservoir computing using diffusive memristors. Adv Intell Syst 1(7):1900084

18. Van der Sande G, Brunner D, Soriano MC (2017) Advances in photonic reservoir computing. Nanophotonics 6(3):561–576
19. Torrejon J et al (2017) Neuromorphic computing with nanoscale spintronic oscillators. Nature 547(7664):428–431
20. Prychynenko D et al (2018) Magnetic skyrmion as a nonlinear resistive element: a potential Building block for reservoir computing. Phys Rev Appl 9(1):014034
21. Scardapane S et al (2017) Advances in biologically inspired reservoir computing. Cogn Comput 9:295–296
22. Liu L et al (2021) Low-Power memristive logic device enabled by controllable oxidation of 2D HfSe2 for In-Memory computing. Adv Sci 8(15):2005038
23. Yin S et al (2019) Emulation of learning and memory behaviors by memristor based on ag migration on 2D MoS2 surface. Phys Status Solidi (a) 216(14):1900104
24. Nagashima K et al (2010) Resistive switching multistate nonvolatile memory effects in a single cobalt oxide nanowire. Nano Lett 10(4):1359–1363
25. Ghafoor F et al (2024) Interface engineering in ZnO/CdO hybrid nanocomposites to enhanced resistive switching memory for neuromorphic computing. J Colloid Interface Sci 659:1–10
26. So H et al (2024) Synaptic properties and Short-Term memory dynamics of TiO2/WOx heterojunction memristor for reservoir computing. Adv Mater Technol 9(5):2301390
27. Park H et al (2024) Long-and Short-Term memory characteristics controlled by electrical and optical stimulations in InZnO-Based synaptic device for reservoir computing. Adv Electron Mater 10(8):2300911
28. Yuan L et al (2021) Organic memory and memristors: from mechanisms, materials to devices. Adv Electron Mater 7(11):2100432
29. Lee S et al (2019) Conducting Bridge resistive switching behaviors in cubic MAPbI3, orthorhombic RbPbI3, and their mixtures. Adv Electron Mater 5(2):1800586
30. Lee S, Son J, Jeong B (2024) Ion dynamics in metal halide perovskites for resistive-switching memory and neuromorphic memristors. Mater Today Electron 9:100114
31. Tian H et al (2017) Extremely low operating current resistive memory based on exfoliated 2D perovskite single crystals for neuromorphic computing. ACS Nano 11(12):12247–12256
32. Nirmal KA et al (2024) Advancements in 2D layered material memristors: unleashing their potential beyond memory. NPJ 2D Mater Appl 8(1):83
33. Mullani NB et al (2023) Surface modification of a titanium carbide Mxene memristor to enhance memory window and low-power operation. Adv Funct Mater 33(26):2300343
34. Hu Z et al (2024) Integration of CeO2-based memristor with vertically aligned nanocomposite thin film: enabling selective conductive filament formation for high-performance electronic synapses. ACS Appl Mater Interfaces 16(47):64951–64962
35. Jeon K et al (2024) Purely self-rectifying memristor-based passive crossbar array for artificial neural network accelerators. Nat Commun 15(1):129
36. Kim M et al (2018) Zero-static power radio-frequency switches based on MoS2 atomristors. Nat Commun 9(1):2524
37. Wang M et al (2018) Robust memristors based on layered two-dimensional materials. Nat Electron 1(2):130–136
38. Shi L et al (2020) Research progress on solutions to the sneak path issue in memristor crossbar arrays. Nanoscale Adv 2(5):1811–1827
39. Yang Q et al (2021) High-performance organic synaptic transistors with an ultrathin active layer for neuromorphic computing. ACS Appl Mater Interfaces 13(7):8672–8681
40. Zhong YN et al (2018) Synapse-like organic thin film memristors. Adv Funct Mater 28(22):1800854
41. Hu S et al (2013) Emulating the paired-pulse facilitation of a biological synapse with a NiOx-based memristor. Appl Phys Lett. https://doi.org/10.1063/1.4804374
42. Zamarreño-Ramos C et al (2011) On spike-timing-dependent-plasticity, memristive devices, and Building a self-learning visual cortex. Front NeuroSci 5:26
43. Feldman DE (2012) The spike-timing dependence of plasticity. Neuron 75(4):556–571
44. Qin J-K et al (2020) Anisotropic signal processing with trigonal selenium nanosheet synaptic transistors. ACS Nano 14(8):10018–10026
45. Shim H et al (2019) Stretchable elastic synaptic transistors for neurologically integrated soft engineering systems. Sci Adv 5(10):eaax4961
46. Wei H et al (2021) Artificial synapses that exploit ionic modulation for perception and integration. Mater Today Phys 18:100329
47. Chen Z et al (2023) All-ferroelectric implementation of reservoir computing. Nat Commun 14(1):3585
48. Choi S et al (2024) 3D-integrated multilayered physical reservoir array for learning and forecasting time-series information. Nat Commun 15(1):2044
49. Farronato M et al (2023) Reservoir computing with charge-trap memory based on a MoS2 channel for neuromorphic engineering. Adv Mater 35(37):2205381
50. Park S-O et al (2022) Experimental demonstration of highly reliable dynamic memristor for artificial neuron and neuromorphic computing. Nat Commun 13(1):2888
51. Xiao H, Rasul K, Vollgraf R (2017) Fashion-mnist: a novel image dataset for benchmarking machine learning algorithms. ArXiv Preprint arXiv:170807747
52. Cohen G et al (2017) *E*MNIST: Extending MNIST to handwritten letters. in. international joint conference on neural networks (IJCNN). 2017. IEEE
53. Deng L (2012) The Mnist database of handwritten digit images for machine learning research [best of the web]. IEEE Signal Process Mag 29(6):141–142
54. Amir A et al (2017) A low power, fully event-based gesture recognition system. in Proceedings of the IEEE conference on computer vision and pattern recognition